HOKKAIDO UNIVERSITY

Title	Optimization of gasoline compression ignition combustion with ozone addition and two-stage direct-injection at middle loads
Author(s)	Kobashi, Yoshimitsu; Dan Da, Tu Dan; Inagaki, Ryuya et al.
Citation	International journal of engine research, 23(2), 232-242 https://doi.org/10.1177/1468087420984574
Issue Date	2022-02-01
Doc URL	https://hdl.handle.net/2115/83734
Rights	Kobashi Y, Dan Da TD, Inagaki R, Shibata G, Ogawa H. Optimization of gasoline compression ignition combustion with ozone addition and two-stage direct-injection at middle loads, International journal of engine research 23(2) pp. 232-242. Copyright © [2022] Institution of Mechanical Engineers (IMechE). DOI: 10.1177/1468087420984574.
Type	journal article
File Information	Manuscript.pdf

1 *Optimization of Gasoline Compression Ignition Combustion with Ozone*
2 *Addition and Two-stage Direct-Injection at Middle Loads*
3
4 Yoshimitsu Kobashi[1]*, Tu Dan Dan Da[1], Ryuya Inagaki[1], G. Shibata[1], H. Ogawa[1]
5
6 [1] Division of Energy and Environmental Systems, Graduate School of Engineering, Hokkaido

7 University, Japan
8

9 **Abstract**

10 Ozone (O_3) was introduced into the intake air to control the ignition in a gasoline

11 compression ignition (GCI) engine. An early fuel injection at -68ºCA ATDC was adopted

12 to mix the fuel with the reactive O-radicals decomposed from the O_3, before the reduction

13 of the O-radicals due to their recombination would take place. The second injection was

14 implemented near top dead center to optimize the profile of the heat release rate. The

15 engine experiments were performed around the indicated mean effective pressure (IMEP)

16 of 0.67 MPa with a primary reference fuel, octane number 90 (PRF90), maintaining the

17 15% intake oxygen concentration with the EGR. The quantity of the first injection, the

18 second injection timing as well as the ozone concentration were changed as experimental

19 parameters. The results showed that the GCI operation with the ozone addition makes it

20 possible to reduce the maximum pressure rise rate while attaining high thermal efficiency,

* Corresponding author at: Kita 13, Nishi 8, Kita-ku, Sapporo, Hokkaido, Japan

E-mail address: kobashi@eng.hokudai.ac.jp   (Yoshimitsu Kobashi)

21 compared to that without the ozone. Appropriate combinations of the ozone concentration

22 and the first injection quantity achieve low smoke and NO_x emissions. Further, the ozone-

23 assisted GCI operation was compared with conventional diesel operation. The results

24 showed that the indicated thermal efficiency of the ozone-assisted GCI combustion is

25 slightly lower than that of the conventional diesel combustion, but that GCI assisted with

26 ozone is highly advantageous to the smoke and NO_x emissions.

27

28 **Keywords:** Gasoline Compression Ignition Engine, Ozone, Two-stage Injection, Thermal

29 Efficiency, Exhaust Emissions

30

31 **Nomenclature**:
32
33 CDC   Conventional diesel combustion
34 GCI   Gasoline compression ignition
35 HCCI   Homogeneous charge compression ignition
36 HTOR   High temperature oxidation reaction
37   "First HTOR" stands for the HTOR of the first injection fuel
38   "Second HTOR" stands for the HTOR of the second injection fuel
39 LTOR   Low temperature oxidation reaction
40 RCCI   Reactivity controlled compression ignition
41 ROHR   Rate of heat release
42 TDC   Top dead center
43
44 $(dp/d\theta)_{max}$ Maximum pressure rise rate [MPa/ºCA]
45 p_{inj} Injection pressure [MPa]
46 $Q_{inj.1st}$ Mass ratio of first injection [%]

47   X_{O3} Concentration of ozone (O_3) in the intake air [ppm]

48

49

50   **Greek symbols:**

51   ϕ_{exh} Exhaust loss [%]

52   ϕ_{other} Other losses [%] equivalent to cooling loss

53   η_i Indicated thermal efficiency [%]

54   η_{comb} Combustion efficiency [%]

55    $\theta_{inj.1st}$ First injection timing [ºCA ATDC]

56    $\theta_{inj.2nd}$ Second injection timing [ºCA ATDC]

57 $\tau_{ign.2nd}$ Ignition delay of second injection [ºCA]

58   **1. Introduction**

59   **1.1 Background**

60   Compression ignition engines offer superior fuel economy. However, in diesel

61   engines, achieving reductions in exhaust emissions remains a problem, as a turbulent

62   diffusion flame surrounds the fuel spray, generating nitrogen oxide (NO_x), and as there is

63   soot formation in the fuel rich central reaction zone [1-2]. The low reactivity of gasoline

64   is advantageous to extend a no flame region between the tip of the fuel injector and the

65   uppermost stream in a turbulent diffusion flame. The length of this zone (from the injector

66   to the flame, elsewhere termed the lift-off length or as here the set-off length) plays a

67   significant role in the soot formation as air is entrained and mixed with the fuel upstream

68   of the set-off length [3-7]. Gasoline has the further benefit to form leaner mixtures due to

69   its high volatility. Considering these features, compression ignition engines using

70   gasoline have attracted increasing attention as alternatives to diesel engines due to the

71   potential for low emissions and high thermal efficiencies [8-11].

72   Unlike homogeneous charge compression ignition (HCCI) in which a homogeneous

73   mixture is ignited, gasoline compression ignition (GCI) is believed to be advantageous to

74   enable better ignition control as the injection is implemented near top dead center (TDC),

75   and as the ignition timing is closely coupled to the injection timing. In practice, however,

76   achieving ignition control over a wide range of engine loads and rotation speeds is

77   challenging as the low reactivity of gasoline increases the dependence of the ignition

78   process of GCI on the time scale of chemical reactions. One approach to control the

79   ignition process of GCI is to employ a multiple-injection strategy, where the fuel injected

80   at an early timing produces reactive radicals, and increases the in-cylinder temperature

81   before TDC, decreasing the ignition delays of the fuel injected subsequently [10-13]. A

82   more effective approach is to introduce reactive chemical species into the intake. Ozone

83   (O_3) may be a potential candidate for this, and it has been investigated for ignition control

84   in HCCI engines [14-18]. Chemical kinetic studies have shown that ozone decomposes

85   at around 600 K, and that O-radicals are generated via the decomposition as follows [19-

86   20]:

87         $O_3 + M = O_2 + O + M$ (R1)
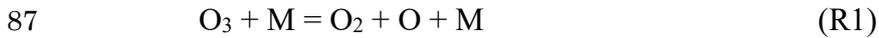
88   The O-radicals reduce the onset temperature of the low temperature heat release, and

89   promote the ignition. The generated O-radicals, however, immediately recombine, to

90   form O_2 as:

91         $O + O + M = O_2 + M$ (R2)
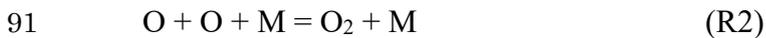
92   This diminishes the impact of the ozone addition on the ignition process of the fuel. The

93   experimental study by Ekoto and Foucher have elucidated the reaction mechanism in a

94   single cylinder engine with an optical diagnostic approach [21].

95   **1.2 Methodology and Purpose of the Present Study**

96   Employing a two-stage injection strategy with an early first injection makes it possible

97   to utilize the reactive O-radicals [22], as shown in Fig.1. (a) The ozone-enriched air is

98   introduced at the intake stroke. (b) The first fuel injection is implemented before the ozone

99   decomposition takes place. (c) The fuel reacts with the O-radicals decomposed from the

100   ozone, and produces reactive radicals. (d) Near TDC, the fuel is injected into the

101   combustion chamber when the reactive radicals are present. This would cause a reactivity

102   stratification in the chamber as proposed in the reactivity controlled compression ignition

103   (RCCI) strategy [23]. The presence of the reactive radicals is advantageous in terms of

104 the combustion efficiency as examined in previous work [24]. A further potential

105 advantage with this strategy is the ability to control ignition delays and set-off length of

106 the second injection, enabling soot formation control.

107   A similar two-stage injection strategy with ozone addition has been proposed by

108 Pinazzi and Foucher aiming to improve low load operation of GCI engines [25], in the

109 present study, however, the GCI operation is extended to higher engine loads.

110   By examining the effects of the ozone concentration and the mass ratio between the

111 first and second injections, the advantage over the conventional GCI combustion is

112 elucidated. Smoke emissions are correlated with the ignition delays of the second

113 injection to evaluate the possibility of set-off length control. Finally, the performance of

114 GCI with the ozone addition is compared with that of diesel combustion employing a high

115 pressure injection strategy.

116 **2. Experimental Setup and Procedures**

117   An illustration of the experimental setup detailed in the previous paper [22] is shown

118 in Fig.2. The test engine was a single cylinder diesel engine equipped with a low pressure

119 EGR pathway and a roots type blower (OGURA CLUTCH, TX04) for supercharging. A

120 common-rail fuel injection system was used, employing a commercially available injector

121   (DENSO, G4S) and an 8-hole nozzle with nominal hole diameters of 0.125 mm and an

122   umbrella angle of 155º. The specifications of the test engine are detailed in Table 1. The

123   bore and stroke are 98 mm and 110 mm, and the displacement volume is 830 cm^3, the

124   compression ratio is 17.6.

125   A piezoelectric pressure sensor (KISTLER, 6125B) was installed in the cylinder head,

126   and the electrical charge produced by the piezoelectric sensor was converted into a

127   voltage signal with a charge amplifier (KISTLER, 5011B). The voltage signal

128   proportional to the cylinder pressure was recorded with a transient memory board at a

129   resolution of 0.2ºCA for 150 cycles.

130   Ozone (O_3) was produced with an ozonizer (EcoDesign, ED-OG-S4AD) while

131   introducing pure oxygen (O_2) from a gas cylinder, and it was delivered into the intake

132   pipe (diameter: 52.7 mm), located 450 mm upstream of the intake port. The volume from

133   the gas inlet to the intake port was larger than the displacement volume, and it was

134   assumed that the ozone-containing oxygen were homogeneously dispersed in the

135   combustion chamber.

136   The ozone concentration was measured with a UV ozone monitor (EBARA, EL-600)

137   before the ozone-containing oxygen was introduced into the intake pipe. The volume-

138   based ozone concentration X_{O3} in the intake air was determined with the measured O_3

139 concentration and the flow rates of the oxygen, and the intake air which was determined

140 using a differential pressure type flowmeter.

141   The concentrations of the total hydrocarbon (THC), carbon monoxide (CO), carbon

142 dioxide (CO_2), nitrogen oxide (NO_x), and oxygen (O_2) were measured at the intake and

143 exhaust pipes with an exhaust gas analyzer (Best Sokki, BEX-5100D). The smoke

144 emissions were measured with a Bosch-type smoke meter (ZEXEL, DSM-20AN).

145   The definitions of the ignition timing and ignition delay of the second injection $\tau_{ign.2nd}$

146 are shown in Fig.3. In most cases in the present study, a two-stage combustion occurred.

147 The first combustion, termed the first HTOR here, is due to the high temperature oxidation

148 reaction (HTOR) of the first fuel injection, and the second, termed the second HTOR, is

149 due to the HTOR of the second fuel injection. The profiles of the rates of heat release

150 (ROHR) due to the first and second HTOR were often overlapping. To determine the

151 ignition timing of the second injection, the ROHR due to the first HTOR (B) was

152 subtracted from the as-recorded ROHR (A), and the ROHR due to the second HTOR (C)

153 was inferred. Assuming a Gaussian distribution in the ROHR profile of the first HTOR,

154 the ROHR profile was inverted at the peak as suggested by the red and green parts of the

155 curves. The ignition timing of the second injection was determined as the derivative of

156 the ROHR of the second injection exceeded 15 J/°CA^2, and the ignition delay of the

157   second injection $\tau_{\text{ign.2nd}}$ was defined to be from the start of the second injection $\theta_{\text{inj.2nd}}$ to

158   the ignition of the fuel introduced in the second injection.

159   **3. Results and Discussion**

160   **3.1 Experimental Conditions**

161   The experimental conditions are detailed in Table 2. The fuel used in the present study

162   is a mixture of primary reference fuels: i-octane (i-C_8H_{18}) and n-heptane (n-C_7H_{16}), and

163   the mixed-in fraction of i-octane in the liquid phase is 90 vol.%, which is termed PRF90,

164   as detailed chemical kinetic models of primary reference fuels have been developed, and

165   it is possible to investigate the effects of chemical reactions due to the ozone addition in

166   the future work.

167   The engine speed was maintained at 1200 rpm. In the previous studies, ozone was

168   applied to improve low load operation of GCI [22, 25]. To examine the benefit of the

169   ozone addition at higher loads, the total injection quantity was set to 29 mg/cycle, and the

170   resultant indicated mean effective pressure (IMEP) was around 0.67 MPa, at the

171   conditions here. As the ozone chemistry mainly affects the low temperature oxidation

172   reaction (LTOR), its interaction depends on the equivalence ratio. It may be interesting to

173   investigate the effects of injection pressure, affecting the equivalence ratio, on the ozone

174   chemistry interaction, but the present study set the injection pressure p_{inj} to 80 MPa,

175   considering the current situation in GCI engines.

176   The ratio of the first injection quantity $Q_{inj.1st}$, defined as the ratio of fuel in the first

177   injection with respect to the total fuel injected, as well as the ozone concentration X_{O3} was

178   changed as the experimental variables, to examine the effects on the ignition timings of

179   the second injection. In the previous study, retarding the first injection timing $\theta_{inj.1st}$

180   decreases the quantity of heat release by the first injection, even remarkable so later than

181   -60ºCA ATDC, showing that the O-radicals decomposed from ozone missed an

182   opportunity to react with the first injection [22]. Considering this and the fact that too

183   early injection may cause wall-wetting, the first injection timing $\theta_{inj.1st}$ was set at -68ºCA

184   ATDC. The second injection timing $\theta_{inj.2nd}$ was advanced from 6ºCA ATDC until the local

185   maximum of the indicated thermal efficiency was identified. The operation was limited

186   by the thresholds of the maximum pressure rise rate $(dp/d\theta)_{max}$ less than 1.0 MPa/ºCA, or

187   when operation became unstable.

188   The intake oxygen concentration, determined to attain NO_x less than 100 ppm in a

189   typical condition, was maintained at 15% with the EGR. By reference to situations in

190   automotive engines at middle loads, the intake air pressure was set at 120 kPa (abs.),

191   maintaining the exhaust gas at the same pressure by throttling the valve at the exhaust

192   pipe. Assuming the increase in the temperature due to the turbocharging, the intake air

193   temperature was set at 60ºC.

194   **3.2 Effects of the Ozone Concentration**

195   Figure 4 shows the profiles of the in-cylinder pressure and rate of heat release

196   (ROHR), changed with the ozone concentration X_{O3}, where the ratio of the first injection

197   quantity $Q_{inj.1st}$ and the second injection timing $\theta_{inj.2nd}$ was set at 35% and at TDC. The

198   small heat release due to the low temperature oxidation reaction (LTOR) of the first

199   injection fuel was identified before -20ºCA ATDC. The heat release appearing near TDC

200   was due to the high temperature oxidation reaction (HTOR) of the first injection fuel (first

201   HTOR), and subsequently the HTOR of the second injection fuel (second HTOR)

202   occurred. With the increase in the ozone concentration X_{O3}, the ROHR in the first HTOR

203   increased, causing an advance in the second HTOR. The ROHR in the second HTOR

204   increased from X_{O3} = 30 ppm to X_{O3} = 60 ppm due to the advanced combustion phasing.

205   A further increase of the ozone concentration decreased the ROHR in the second HTOR

206   due to the decreased ignition delay of the second injection, coupled with the effects of the

207   decrease in fuel available for the second HTOR.

208   Figure 5 shows the indicated thermal efficiency η_i, combustion efficiency η_{comb},

209 exhaust loss ϕ_{exh}, and other losses ϕ_{other} at the fixed ratio of the first injection quantity

210 $Q_{inj.1st}$ of 35%. Here, the other losses ϕ_{other} are equivalent to the cooling loss. The

211 combustion efficiency was improved with the increase in the ozone concentration X_{O3}. As

212 the source of the unburned emissions may be the lean mixture formed by the first injection,

213 this result suggests that the ozone addition improves the reactivity of the lean mixture.

214 The retarded second injection timing $\theta_{inj.2nd}$ deteriorated the combustion efficiency, and

215 increased the exhaust loss due to the retarded combustion phasing. With the increase in

216 the ozone concentration X_{O3}, the combustion phasing advanced as seen in Fig.4, followed

217 by a decrease in the exhaust loss, and an increase in the other losses. As the balance

218 between these effects, the maximum indicated thermal efficiency was achieved with X_{O3}

219 = 60 ppm and 120 ppm.

220 **3.3 Effects of the Ratio of the First Injection Quantity**

221 Figure 6 shows the profiles of the rate of heat release (ROHR), changed with the

222 second injection timing $\theta_{inj.2nd}$, for different ratios of the first injection quantity $Q_{inj.1st}$.

223 Here, the ozone concentration X_{O3} attaining high thermal efficiency was selected with

224 respect to each $Q_{inj.1st}$. The experiments were implemented under the following

225 conditions; 120, 180, 240, 300, and 360 ppm for the $Q_{inj.1st}$ of 20%; 30, 60, 120, and 180

226   ppm for the $Q_{inj.1st}$ of 35%; 10, 30, 60, and 120 ppm for the $Q_{inj.1st}$ of 50%; 0, 10, and 30

227   ppm for the $Q_{inj.1st}$ of 60%, while changing the second injection timing. These conditions

228   were chosen to find local maximum values of the indicated thermal efficiency with

229   respect to the change in the ozone concentration. In the case of the $Q_{inj.1st}$ of 60%, there

230   was no significant differences in the maximum indicted thermal efficiency between the

231   ozone concentrations X_{O3}, so that $X_{O3} = 0$ ppm was selected here for a comparison purpose.

232   The X_{O3} decreased with the increase of the $Q_{inj.1st}$ from 300 ppm to 0 ppm, and stable GCI

233   operation without ozone ($X_{O3} = 0$ ppm) were achieved with the $Q_{inj.1st}$ of 60%. The second

234   injection timing $\theta_{inj.2nd}$ achieving the maximum indicated thermal efficiency is that

235   underlined in the figure.

236   The late combustion phasing was identified with the ratio of the first injection quantity

237    $Q_{inj.1st}$ of 20%. This is because the ROHR in the first HTOR, which occurred near TDC,

238   was very small. The ROHR in the first HTOR increased with the increase in the first

239   injection $Q_{inj.1st}$ from 20% to 50%, advancing the second HTOR. With the $Q_{inj.1st}$ at 60%,

240   in the absence of ozone, the first HTOR occurred after TDC, and the first and second

241   injection fuels burned simultaneously with the second injections before the $\theta_{inj.2nd}$ of TDC,

242   causing the sudden elevation in the ROHR.

243   Figure 7 shows the indicated thermal efficiency η_i, combustion efficiency η_{comb},

244 exhaust loss ϕ_{exh}, and other losses ϕ_{other} for different ratios of the first injection quantity

245 $Q_{inj.1st}$. The data shown in this figure were acquired under experimental conditions

246 identical to those in Fig.6, except for the data acquired at the $Q_{inj.1st}$ of 60% and $\theta_{inj.2nd}$ of

247 -4ºCA ATDC, which is added to show the trend including the knocking condition.

248 The advance of the second injection improved the indicated thermal efficiency as the

249 combustion phasing was advanced, and the exhaust loss decreased. The $Q_{inj.1st}$ of 60%

250 achieved the lowest exhaust loss as the combustion phasing was early (see Fig.6), and

251 combustion periods were shorter than the others. The combustion efficiency with the

252 $Q_{inj.1st}$ of 60% was lower than that with the $Q_{inj.1st}$ of 35% and 50% due to the absence of

253 ozone. With the $Q_{inj.1st}$ of 60%, a further increase of the ozone concentration can increase

254 the combustion efficiency and thermal efficiency at the second injection timings later than

255 TDC, but the combustion phasing would be too far advanced against the early second

256 injection timings, causing deterioration of the thermal efficiency. A further increase of the

257 ozone concentration along with decreases of the intake oxygen concentration and intake

258 air pressure may be a possible way to increase the combustion efficiency and to optimize

259 the combustion phasing for the early second injections. With the $Q_{inj.1st}$ of 20%, the late

260 combustion phasing deteriorated the combustion efficiency and exhaust loss, and caused

261 the unstable operation, while advancing the second injection improved the combustion

262 efficiency due to the advanced combustion phasing, coupled with the combustion

263 enhancement effects induced by the higher concentration of ozone.

264 The $Q_{inj.1st}$ of 60% yielded the higher other losses value. The larger quantity in the

265 first injection may increase the cooling loss as the combustion temperature of the mixture

266 which is widely spread throughout the combustion chamber increases. In addition, the

267 rapid combustion of the $Q_{inj.1st}$ of 60% may increase the cooling loss due to increased wall

268 heat transfer. The other losses with the $Q_{inj.1st}$ of 50% were slightly higher than that with

269 the $Q_{inj.1st}$ of 35%, but the differences were rather small, and increased from $Q_{inj.1st}$ of 35%

270 to 20%. This may be because the momentum of the spray flame increased with the

271 increase of the second injection quantity, and more of the spray flame impinged on the

272 piston wall, enhancing the heat transfer to the wall.

273 Overall, this suggests that with the $Q_{inj.1st}$ of 35% and 50%, the higher combustion

274 efficiency and lower cooling loss are advantageous to the indicated thermal efficiency η_i.

275 With the $Q_{inj.1st}$ of 60%, the lower exhaust loss is advantageous to the indicated thermal

276 efficiency η_i. The combustion efficiency with the $Q_{inj.1st}$ of 60% is improved with the

277 advanced second injection, but the knocking limits the improvements.

278 Figure 8 plots the maximum pressure rise rate $(dp/d\theta)_{max}$ for different ratios of the

279 first injection quantity $Q_{inj.1st}$. The experiments were performed under the conditions in

280   Fig.7. At the second injection timings $\theta_{inj.2nd}$ before 2ºCA ATDC, the maximum pressure

281   rise rate with the $Q_{inj.1st}$ at 60% was the highest, followed by that with the $Q_{inj.1st}$ at 35%,

282   50%, and 20%, decreasing in this order. With the $Q_{inj.1st}$ at 60%, the heat release due to

283   the first and second HTOR overlap as the second injection timing advances, resulting in

284   the increase of the ROHR seen in Fig.6. The maximum pressure rise rate with the $Q_{inj.1st}$

285   of 20% was lower than the others due to the late combustion, but here a further advance

286   in the second injection was limited by the appearance of knocking. As the amount of the

287   heat release in the first HTOR was small (see Fig.6), the ignition delay of the second

288   injection was long, and a somewhat large amount of fuel remained until the second HTOR.

289   This causes a large heat release with the advance of the combustion phase associated with

290   the advanced second injection. Overall, this suggests that an appropriate amount of heat

291   release due to the first HTOR is necessary to control the maximum pressure rise rate as

292   with the $Q_{inj.1st}$ of 35% and 50%.

293   **3.4 Comparison of the Impact of Ozone Concentration and Ratio of Fuel Injection**

294   **Quantity under the Optimized Conditions**

295   Figure 9 shows the relation among the combustion efficiency η_{comb}, ozone

296   concentration X_{O3}, and the ratio of the first injection quantity $Q_{inj.1st}$. For all the data shown

297   here, the second injection timings achieving the maximum indicated thermal efficiency

298   were selected. It can be seen clearly that the combustion efficiency increases with the

299   increase of the ozone concentration for each level of the ratio of the first injection quantity.

300   Figure 10 shows the relation among the indicated thermal efficiency η_i, ozone

301   concentration X_{O3}, and the ratio of the first injection quantity $Q_{inj.1st}$. As in Fig.9, the

302   second injection timings achieving the maximum indicated thermal efficiency were

303   selected. The ozone concentration achieving the maximum indicated thermal efficiency

304   decreased with the increase in the $Q_{inj.1st}$. The indicated thermal efficiency increases with

305   the increase of the ozone concentration due to the increased combustion efficiency, but it

306   decreases when the ozone concentration exceeds a certain level. This trend can be

307   observed for each level of the ratio of the first injection quantity. This is due to a

308   combustion phasing advancement and increased cooling loss. There were very limited

309   differences in the maximum indicated thermal efficiency from the $Q_{inj.1st}$ of 35% to 60%.

310   Recall that, however, in the case of $Q_{inj.1st}$ of 60%, the operation achieving high indicated

311   thermal efficiency was accompanied by the high $(dp/d\theta)_{max}$.

312   Figure 11 shows the relation among the exhaust emissions, ozone concentrations X_{O3},

313   and the ratio of the first injection quantity $Q_{inj.1st}$. The smoke and NO_x emissions increased

314   with increases in the X_{O3} and the $Q_{inj.1st}$. Increases in the X_{O3} and $Q_{inj.1st}$ increased the heat

315   release in the first HTOR, and advanced the timing of the first HTOR, increasing the in-

316   cylinder gas temperature and the NO_x formation rate. Figure 12 shows the smoke

317   concentration vs. the ignition delay of the second injection $\tau_{ign.2nd}$, where all the data

318   acquired in the present experiments are plotted. The data acquired under the same

319   conditions as in Fig.11 are shown as filled (solid) symbols. Where the ignition delay was

320   difficult to determine, when there was simultaneous ignition of the first and second

321   injections, the experiment data is not plotted in the figure. The smoke emissions occurred

322   with the $\tau_{ign.2nd}$ shorter than 6ºCA; as the larger quantity of the first injection resulted in

323   the shorter $\tau_{ign.2nd}$, the smoke emissions increased with the increase of the X_{O3} and $Q_{inj.1st}$.

324   **3.5 Comparison with Conventional Diesel Combustion**

325   The engine performance and the exhaust emissions of GCI with the ozone addition

326   are next compared with those of conventional diesel combustion (CDC). The

327   experimental conditions of the conventional diesel combustion are detailed in Table 3.

328   The total injection quantity is slightly increased compared to the PRF90, to correct the

329   differences in the lower heating values. The other conditions were identical to those in

330   Table 2. As a preliminary experiment, the injection timings and the pilot injection amount

331   which achieved the maximum indicated thermal efficiency were determined while

332   maintaining the crank angle interval between the pilot and main injections at 8ºCA at the

333   injection pressure p_{inj} of 80 MPa, at this condition the injection pressure was then changed

334   from 80 MPa to 200 MPa, without other changes in the experimental conditions.

335   Figure 13 plots the profiles of the ROHR between GCI with the ozone addition and

336   CDC with the different injection pressures. The operation with the $Q_{inj.1st}$ of 35%, the X_{O3}

337   of 60 ppm, and the $\theta_{inj.2nd}$ of TDC was selected as the best GCI condition in this study.

338   Compared at the p_{inj} of 80 MPa, GCI with the ozone addition presented a ROHR that was

339   higher than CDC, representing the premixed combustion nature. The increase of the p_{inj}

340   in CDC increased the ROHR of the pilot and main injections, reducing the combustion

341   periods.

342   Figure 14 shows the indicated thermal efficiency η_i of CDC, compared with the best

343   GCI operations derived from Fig.10. Compared at the same injection pressure of 80 MPa,

344   the differences of the indicated thermal efficiency between CDC and GCI with the $Q_{inj.1st}$

345   of 35% and 60% are smaller than 1%, but increased with the increase of the injection

346   pressure of CDC.

347   Figure 15 shows the trade-off relationship between the smoke and NO_x emissions.

348   Here, the data shown in Fig.11 are plotted for comparison purposes. CDC with the

349   injection pressure of 80 MPa generated the very high smoke concentration as well as the

350 slightly higher NO_x. Increasing the injection pressure up to 200 MPa in CDC, the smoke

351 decreased dramatically, accompanied by the increase of NO_x. This result demonstrates

352 that GCI assisted by ozone offers operation with the very low smoke and NO_x emissions.

353 **4. Conclusions**

354 The present study added ozone (O_3) to a gasoline compression ignition (GCI) engine,

355 aiming to control the ignition timing and combustion progress. A two-stage fuel injection

356 with very early injection and late injection close to top dead center was adapted to utilize

357 O-radicals decomposed from the O_3 before the recombination reaction reduces them to

358 O_2. The first injection quantity, the second injection timing as well as the O_3 concentration

359 were varied to explore the optimum operation conditions at medium loads with a single

360 cylinder GCI engine. Further, the engine performance and exhaust emissions with GCI

361 were compared with conventional diesel combustion operation. The conclusions may be

362 summarized as follows:

363 1. The GCI operation with a smaller amount of first injection results in combustion with

364 lower combustion efficiency, so that higher ozone concentrations are required to

365 increase combustion efficiency and to attain higher indicated thermal efficiency.

366 2. For each level of the ratio of the first injection quantity, with the increase of the ozone

367   concentration, the combustion efficiency increases, and the combustion phasing

368   advances, accompanied by the increase of the cooling loss. Due to the balance

369   between the combustion efficiency and the cooling loss, he indicated thermal

370   efficiency has a local maximum value with respect to the ozone concentration.

371 3. The GCI operation without ozone is accompanied by a higher maximum pressure rise

372   rate due to the simultaneous ignition of the first and second injection fuels. With an

373   appropriate amount of first injection and ozone addition, the high temperature

374   oxidation reactions of the first and second injection fuels occur in two stages,

375   decreasing the maximum pressure rise rate.

376 4. The increase of the ozone concentration and the first injection quantity increase the

377   rate of heat release caused by the high temperature oxidation of the first injection fuel.

378   This increases the in-cylinder temperature and NO_x emissions, and decreases the

379   ignition delay of the second injection, accompanied by the increase of the smoke

380   emissions.

381 5. The indicated thermal efficiency of GCI assisted with ozone is slightly lower than that

382   of the conventional diesel combustion, but GCI assisted with ozone is advantageous

383   to the smoke and NO_x emissions.

384

385   The present study produced O_3 from pure oxygen on a trial basis. According to the

386   previous study by Inoue et al. who developed an intake in-line ozonizer, the ozone

387   enrichment in the order of 60 ppm is technically viable with air [26]. Estimated by

388   reference to this study [26], the energy loss due to the ozone production is about 1% in

389   the engine operation condition employed in this study. Further improvements in the

390   efficiency are still required.

391   **Acknowledgements**

394

395   **5. References**

396   [1] Dec, J. E., "A Conceptual Model of DI Diesel Combustion Based on Laser-Sheet
397   Imaging," SAE Technical Paper, No.970873, 1997.
398   [2] Kosaka, H., Aizawa, T. and Kamimoto, T., "Two-dimensional Imaging of Ignition and
399   Soot Formation Processes in a Diesel Flame," International Journal of Engine
400   Research, Vol.6, Issue 1, pp.21-42, 2005.
401   [3] Siebers, D. and Higgins, B., "Flame Lift-Off on Direct-Injection Diesel Sprays under
402   Quiescent Conditions," SAE Technical Paper 2001-01-0530, 2001.
403   [4] Higgins, B. and Siebers, D., "Measurement of the Flame Lift-Off Location on DI
404   Diesel Spray using OH Chemiluminescence," SAE Technical Paper 2001-01-0918,
405   2001.

406 [5] Siebers, D., Higgins, B. and Pickett, L., "Flame Lift-Off on Direct-Injection Diesel
407   Fuel Jets: Oxygen Concentration Effects," SAE Technical Paper 2002-01-0890, 2002.
408 [6] Pickett, L., Siebers, D. and Idicheria, C., "Relationship between Ignition Processes
409   and the Lift-Off Length of Diesel Fuel Jets," SAE Technical Paper 2005-01-3843,
410   2005.
411 [7] Yasutomi, K., Mueller, C. J., Pickett, L. M. and Skeen, S. A., "Investigation of the
412   Spray and Combustion Characteristics of Four Multi-Component Diesel Surrogates
413   Fuels Relative to Their Commercial Target Fuel," THIESEL 2018 Conference on
414   Thermo- and Fluid Dynamic Processes in Direct Injection Engines, 2018.
415 [8] Kalghatgi, G., Risberg, P., and Ångström, H., "Advantages of Fuels with High
416   Resistance to Auto-ignition in Late-injection, Low-temperature, Compression
417   Ignition Combustion," SAE Technical Paper 2006-01-3385, 2006.
418 [9] Kalghatgi, G., Risberg, P., and Ångström, H., "Partially Pre-Mixed Auto-Ignition of
419   Gasoline to Attain Low Smoke and Low NOx at High Load in a Compression Ignition
420   Engine and Comparison with a Diesel Fuel," SAE Technical Paper 2007-01-0006,
421   2007.
422 [10] Hanson, R., Splitter, D., and Reitz, R., "Operating a Heavy-Duty Direct Injection
423   Compression-Ignition Engine with Gasoline for Low Emissions," SAE Technical
424   Paper 2009-01-1442, 2009.
425 [11] Manente, V., Johansson, B., and Cannella, W., "Gasoline Partially Premixed
426   Combustion, the Future of Internal Combustion Engines?," International Journal of
427   Engine Research, Vol.12, Issue 3, pp.194-208, 2011.
428 [12] Ra, Y., Loeper, P., Andrie, M., Krieger, R., Foster, D., Reitz, R., and Durrett, R.,
429   "Gasoline DICI Engine Operation in the LTC Regime Using Triple-pulse Injection,"
430   SAE Int. J. Engines 5(3), 2012.
431 [13] Sellnau, M. C., Sinnamon, J., Hoyer, K., and Husted, H., "Full-time Gasoline Direct-
432   injection Compression Ignition (GDCI) for High Efficiency and Low NOx and PM,"
433   SAE Int. J. Engines 5(2), 2012.
434 [14] Nishida, H. and Tachibana, T., "Homogeneous Charge Compression Ignition of
435   Natural Gas/Air Mixture with Ozone Addition," Journal of Propulsion and Power,
436   Vol.22, No.1, pp.151-157, 2006.
437 [15] Mohammadi, A., Kawanabe, H., Ishiyama, T., Shoji M. and Komada, A., "Study on
438   Combustion Control in Natural-Gas PCCI Engines with Ozone Addition into Intake
439   Gas," SAE Technical Paper 2006-01-0419, 2006.
440 [16] Schönborn, A., Hellier, P., Aliev, A E. and Ladommatos, N., "Ignition Control of
441   Homogeneous-Charge Compression Ignition (HCCI) Combustion Through

442   Adaptation of the Fuel Molecular Structure by Reactions with Ozone," Fuel, Vol.89,
443   Issue 11, pp.3178-3184, 2010.

444 [17] Foucher, F., Higelin, P., Mounaïm-Rousselle, C. and Dagaut, P., "Influence of Ozone
445   on the Combustion of n-heptane in a HCCI Engine," Proc. the Combustion Institute,
446   Vol.34, Issue 2, pp.3005-3012, 2013.

447 [18] Masurier, J.-B., Foucher, F., Dayma, G. and Dagaut, P., "Investigation of iso-Octane
448   Combustion in a Homogeneous Charge Compression Ignition Engine Seeded by
449   Ozone, Nitric Oxide and Nitrogen Dioxide," Proc. the Combustion Institute, Vol.35,
450   Issue 3, pp.3125-3132, 2015.

451 [19] Heimerl, J. M. and Coffee, T. P., "The Detailed Modeling of Premixed, Laminar
452   Steady-State Flames. I. Ozone," Combustion and Flame, Vol.39, Issue 3, pp.301-315,
453   1980.

454 [20] Yamada, H., Yoshii, M. and Tezaki, A., "Chemical Mechanistic Analysis of Additive
455   Effects in Homogeneous Charge Compression Ignition of Dimethyl Ether," Proc. the
456   Combustion Institute, Vol.30, Issue 2, pp.2773-2780, 2005.

457 [21] Ekoto, I. and Foucher, F., "Mechanisms of Enhanced Reactivity with Ozone Addition
458   for Advanced Compression Ignition," SAE Technical Paper 2018-01-1249, 2018.

459 [22] Kobashi, Y., Wang, Y., Shibata, G., Ogawa, H. and Naganuma, K., "Ignition Control
460   in a Gasoline Compression Ignition Engine with Ozone Addition Combined with a
461   Two-stage Direct-injection Strategy," Fuel, Vol.249, pp.154-160, 2019.

462 [23] Kokjohn, S. L., Hanson, R. M., Splitter, D. A. and Reitz, R. D., "Fuel Reactivity
463   Controlled Compression Ignition (RCCI): A Pathway to Controlled High-Efficiency
464   Clean Combustion," International Journal of Engine Research, Vol.12, Issue 3,
465   pp.209-226, 2011.

466 [24] Kobashi, Y., Tanaka, D., Maruko, T., Kato, S., Kishiura, M., and Senda, J., "Effects
467   of Mixedness and Ignition Timings on PCCI Combustion with a Dual Fuel
468   Operation," SAE Technical Paper 2011-01-1768, 2011.

469 [25] Pinazzi, P. M. and Foucher, F., "Potential of Ozone to Enable Low Load Operations
470   of a Gasoline Compression Ignition (GCI) Engine," SAE Technical Paper 2017-01-
471   0746, 2017.

472 [26] Inoue, T., Tamida, T., Hashimoto, T., Wada, N., Nakagawa, A., Sakashita, T., Wada,
473   K. and Honda, T., "The development of intake in-line type ozonizer for application
474   to HCCI combustion", Transactions of Society of Automotive Engineers of Japan,
475   Vol.48, No.4 (2017), pp.827-832 (in Japanese).

Table 1 Specifications of the test engine

Bore x Stroke [mm]		98 x 110
Displacement [cm^3]		830
Compression ratio [-]		17.6
Injection nozzle	Spray included angle [º]	155
	Number of nozzle hole	8
	Nozzle hole diameter [mm]	0.125

Table 2 Experimental conditions for gasoline compression ignition (GCI) with ozone addition

Fuel	PRF90
Engine rotation speed [rpm]	1200
Intake oxygen concentration [%]	15
Intake air temperature [ºC]	60
Intake air pressure [kPa (abs.)]	120
Intake O_3 concentration X_{O3} [ppm]	0 to 360
Fuel injection pressure p_{inj} [MPa]	80
First injection timing $\theta_{inj.1st}$ [ºCA ATDC]	-68
Second injection timing $\theta_{inj.2nd}$ [ºCA ATDC]	-6 to 6
Ratio of first injection quantity $Q_{inj.1st}$ [%]	20 to 60
Total injection quantity [mg]	29
IMEP [MPa]	≈ 0.67

Table 3　Experimental conditions for conventional diesel combustion (CDC)

Fuel	JIS No.2 Diesel fuel
Fuel injection pressure　p_{inj} [MPa]	80, 120, 160, 200
Pilot injection timing　$\theta_{inj.1st}$ [ºCA ATDC]	-10
Main injection timing　$\theta_{inj.2nd}$ [ºCA ATDC]	-2
Pilot injection quantity [mg]	1
Main injection quantity [mg]	29

1

2 Air w/ O₃   Fuel→   Fuel→

3

4   Air w/ O_2 + O   Air w/Reactive

5   Air w/ O_3 Air w/ O_3 Fuel + O   radicals

6

7

8   (a)   (b)   (c)   (d)

9
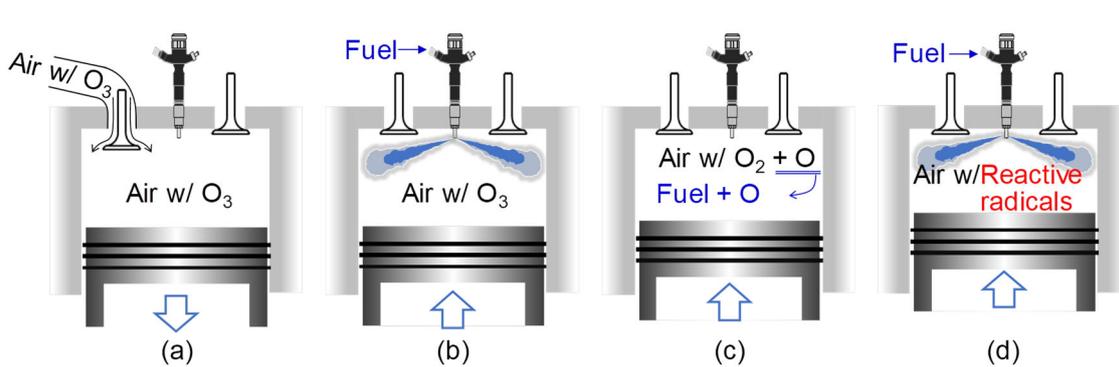
10 Figure 1 Schematic of the combustion control methodology with ozone addition and two-
stage injection, proposed in this study

11
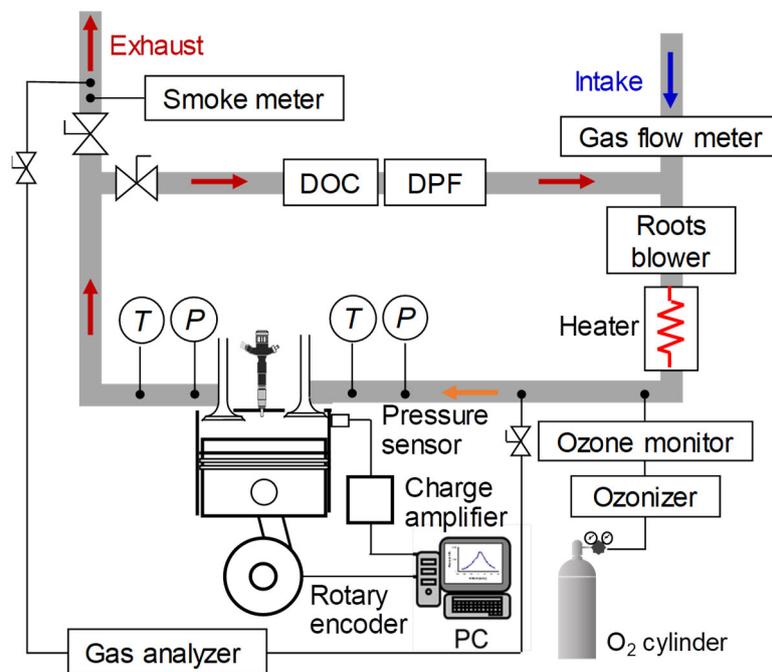
Figure 2 Illustration of the experimental setup

1
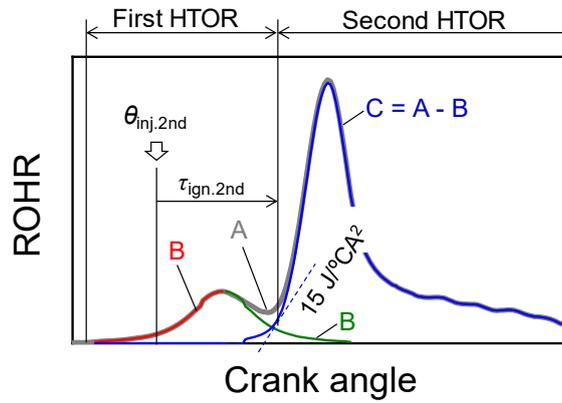
Figure 3 Definition of the ignition delay of the second injection
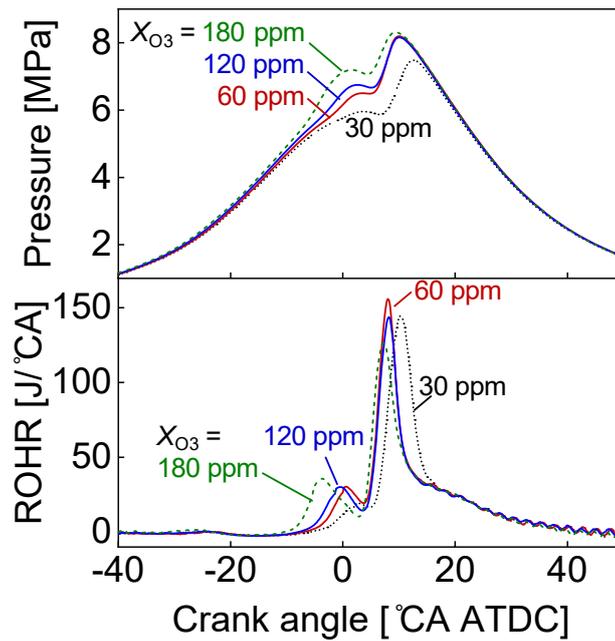
Figure 4 Profiles of the in-cylinder pressure and rate of heat release (ROHR), changing with the ozone concentration X_{O3} ($Q_{inj.1st} = 35\%$, $\theta_{inj.2nd} = $ TDC)
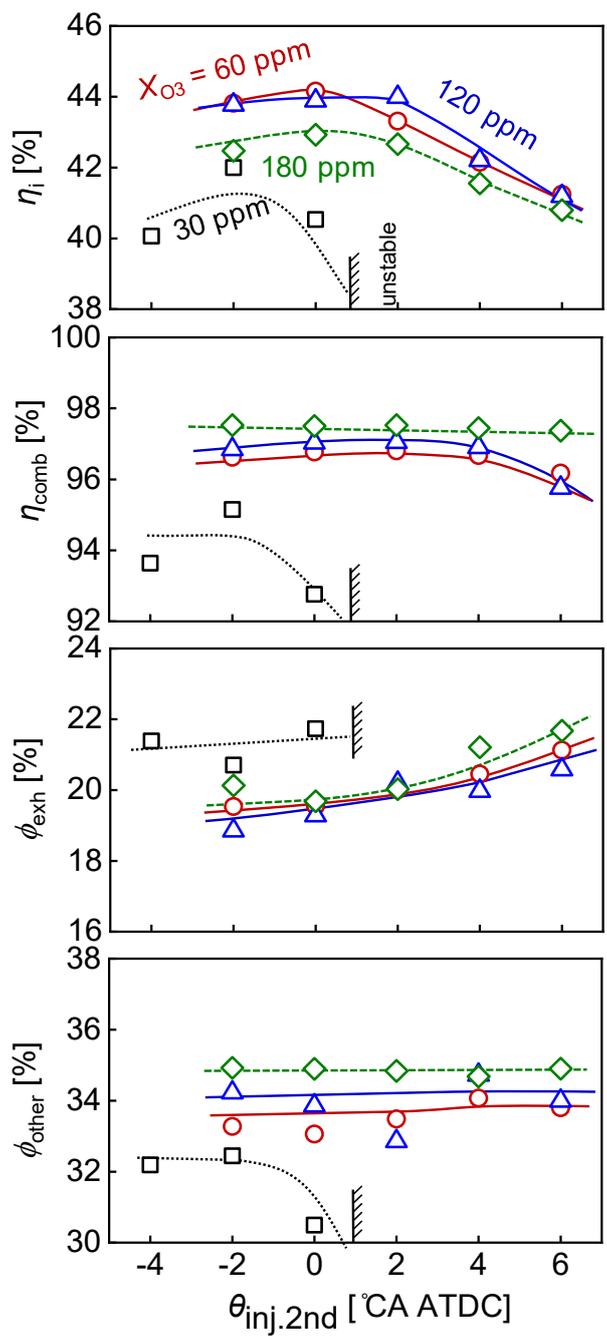
Figure 5 Effects of the ozone concentration X_{O3} on the indicated thermal efficiency η_i, combustion efficiency η_{comb}, exhaust loss ϕ_{exh}, and other loss ϕ_{other} ($Q_{inj.1st} = 35\%$)
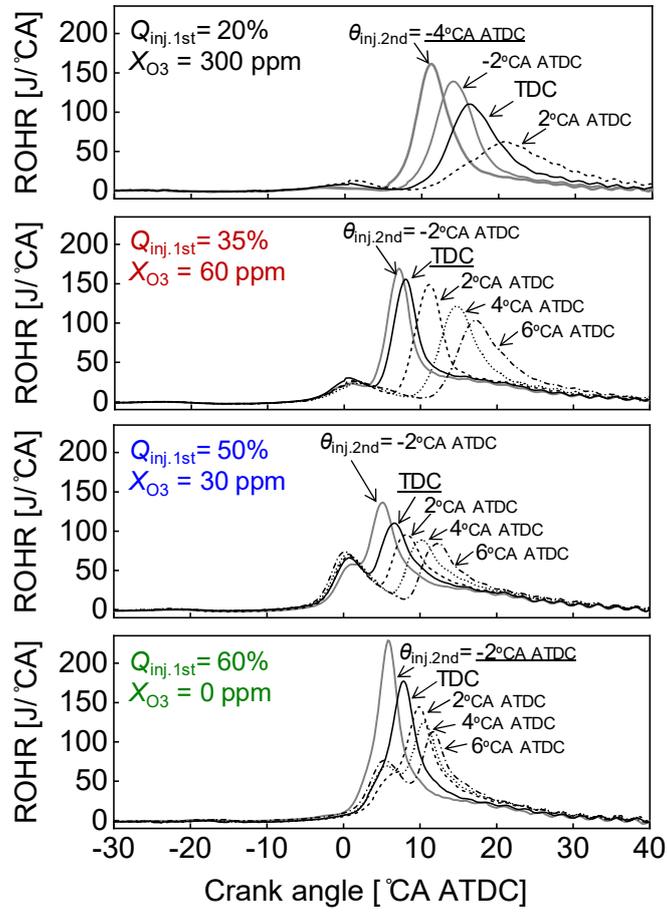
Figure 6 Profiles of the rate of heat release (ROHR), changing with the second injection timing $\theta_{inj.2nd}$

Ozone concentrations achieving high indicated thermal efficiency were selected

145
146
147
148
149
150
151
152
153
154
155
156
157
158
159
160
161
162
163
164
165
166
167
168
169
170
171
172
173
174
175
176
177
178
179
180
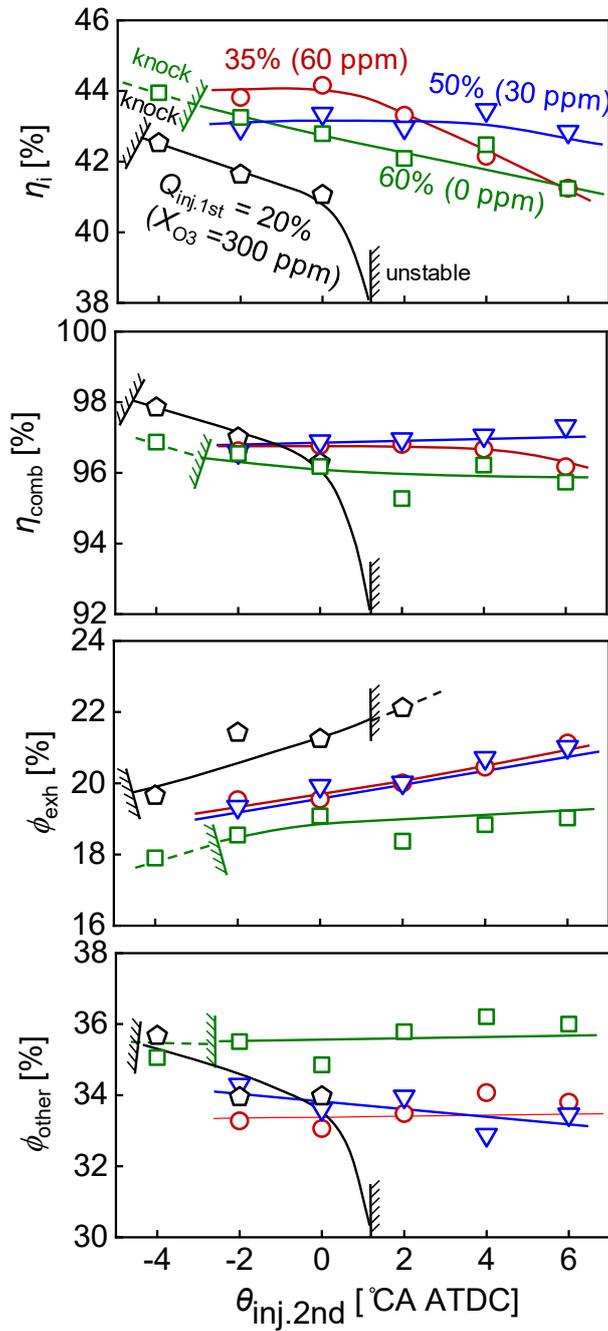
Figure 7 Comparison of the indicated thermal efficiency η_i, combustion efficiency η_{comb}, exhaust loss ϕ_{exh}, and other losses ϕ_{other} between the ratio of the first injection quantity $Q_{inj.1st}$
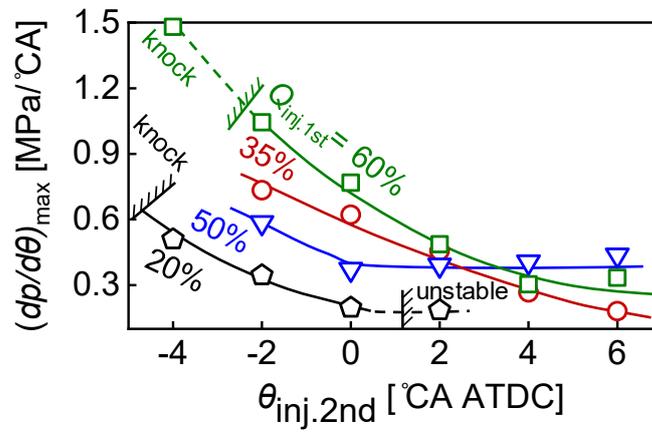
Figure 8 Comparison of the maximum pressure rise rate between the ratio of
the first injection quantity $Q_{\text{inj.1st}}$
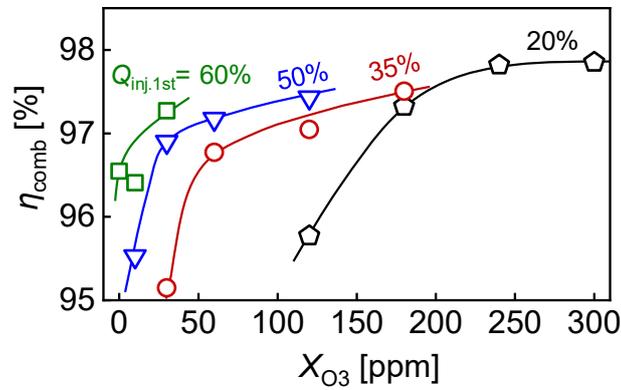
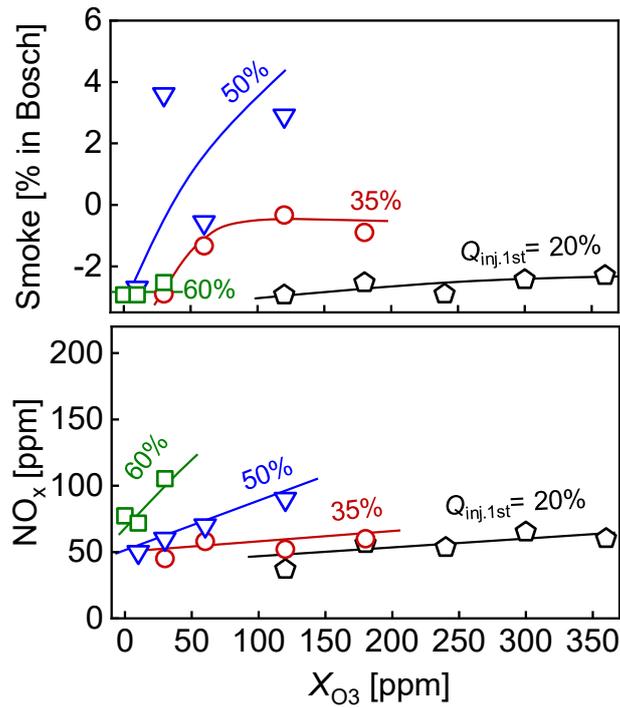Figure 9   Effects of the ozone concentration X_{O3} and the ratio of the first injection quantity $Q_{inj.1st}$ on the combustion efficiency η_{comb}

The second injection timings achieving the maximum indicated thermal efficiency were selected
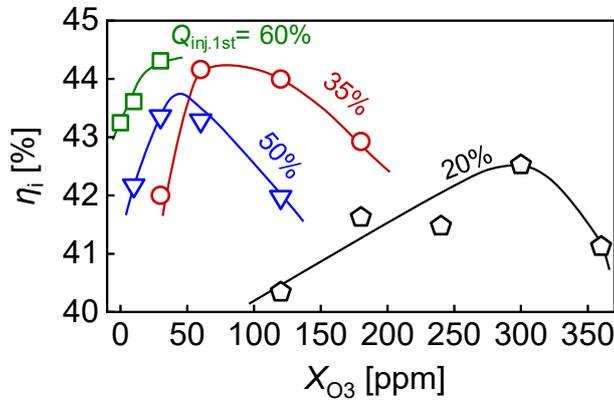
Figure 10   Effects of the ozone concentration X_{O3} and the ratio of the first injection quantity $Q_{inj.1st}$ on the indicated thermal efficiency η_i

The second injection timings achieving the maximum indicated thermal efficiency were selected

Figure 11   Effects of the ozone concentration X_{O3} and the ratio of the first injection quantity $Q_{inj.1st}$ on the smoke and NOx emissions
The second injection timings achieving the maximum indicated thermal efficiency were selected
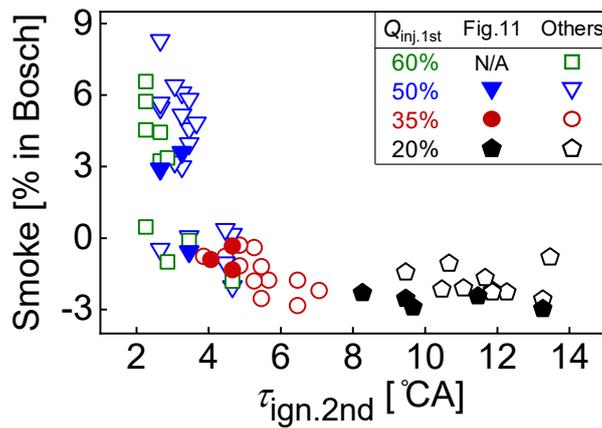

Figure 12   Smoke concentration vs. the ignition delay of the second injection $\tau_{ign.2nd}$
All the data points, except for the conditions where the ignition delay was difficult to determine (due to overlapping), were plotted

289
290
291
292
293
294
295
296
297
298
299
300
301
302
303
304
305
306
307
308
309
310
311
312
313
314
315
316
317
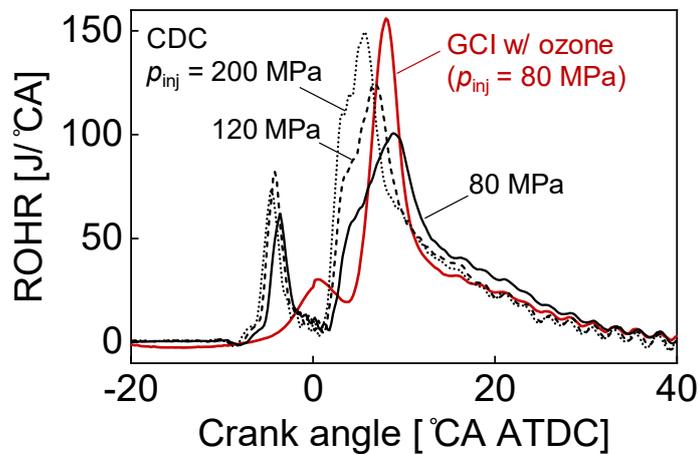318
319
320
321
322
323
324

Figure 13   Comparison of profiles of the rate of heat release (ROHR) between the gasoline compression ignition (GCI) with ozone addition and conventional diesel combustion (CDC) with different injection pressures p_{inj}
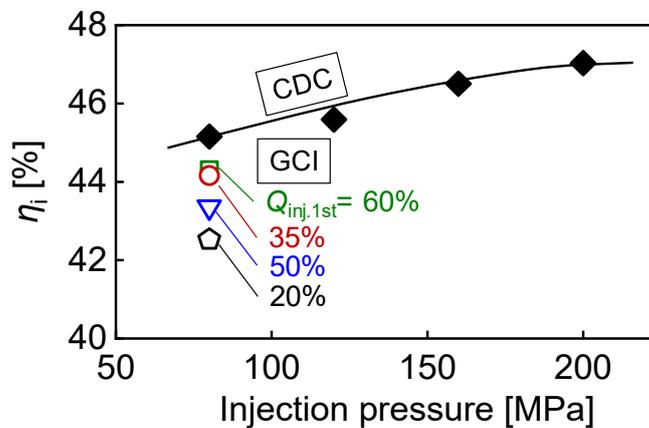

Figure 14   Comparison of the indicated thermal efficiency η_i between the gasoline compression ignition (GCI) with ozone addition and conventional diesel combustion (CDC) with different injection pressures p_{inj}
The GCI data were derived from Fig.10, selecting the maximum indicated thermal efficiency with respect to each of the quantities of the first injection

325
326
327
328
329
330
331
332
333
334
335
336
337
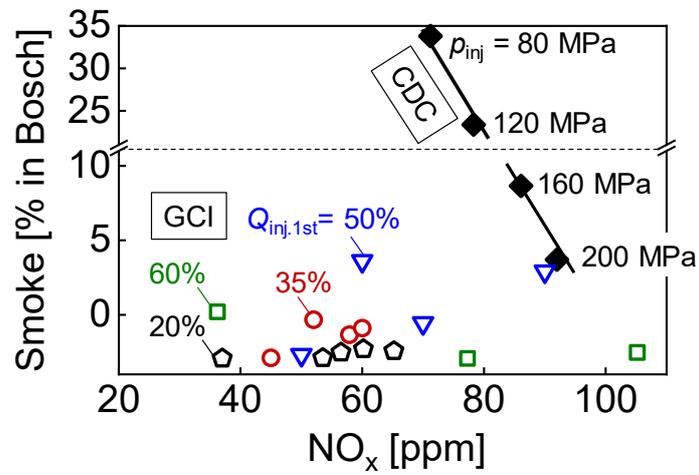338
339
340
341
342
343
344
345
346
347
348
349

Figure 15   Comparison of the smoke and NO_x emissions between the gasoline compression ignition (GCI) with ozone addition and conventional diesel combustion (CDC) with different injection pressures p_{inj}
The GCI data were derived from Fig.11